



**HAL**  
open science

## Translational and Rotational Dynamical Heterogeneities in Granular Systems

Binquan Kou, Yixin Cao, Jindong Li, Chengjie Xia, Zhifeng Li, Haipeng  
Dong, Ang Zhang, Jie Zhang, Walter Kob, Yujie Wang

► **To cite this version:**

Binquan Kou, Yixin Cao, Jindong Li, Chengjie Xia, Zhifeng Li, et al.. Translational and Rotational Dynamical Heterogeneities in Granular Systems. *Physical Review Letters*, 2018, 121, pp.018002-1. 10.1103/PhysRevLett.121.018002 . hal-01833984

**HAL Id: hal-01833984**

**<https://hal.science/hal-01833984>**

Submitted on 2 Jun 2021

**HAL** is a multi-disciplinary open access archive for the deposit and dissemination of scientific research documents, whether they are published or not. The documents may come from teaching and research institutions in France or abroad, or from public or private research centers.

L'archive ouverte pluridisciplinaire **HAL**, est destinée au dépôt et à la diffusion de documents scientifiques de niveau recherche, publiés ou non, émanant des établissements d'enseignement et de recherche français ou étrangers, des laboratoires publics ou privés.



Distributed under a Creative Commons Attribution 4.0 International License

# Translational and rotational dynamical heterogeneities in granular systems

Binquan Kou,<sup>1</sup> Yixin Cao,<sup>1</sup> Jindong Li,<sup>1</sup> Chengjie Xia,<sup>1</sup> Zhifeng Li,<sup>1</sup> Haipeng Dong,<sup>2</sup> Ang Zhang,<sup>2</sup> Jie Zhang,<sup>1,3</sup> Walter Kob,<sup>4,\*</sup> and Yujie Wang<sup>1,5,6,†</sup>

<sup>1</sup>*School of Physics and Astronomy, Shanghai Jiao Tong University,  
800 Dong Chuan Road, Shanghai 200240, China*

<sup>2</sup>*Department of Radiology, Ruijin Hospital, Shanghai Jiao Tong University School of Medicine, Shanghai 200025, China*

<sup>3</sup>*Institute of Natural Sciences, Shanghai Jiao Tong University, Shanghai 200240, China*

<sup>4</sup>*Laboratoire Charles Coulomb, University of Montpellier and CNRS, Montpellier 34095, France*

<sup>5</sup>*Materials Genome Initiative Center, Shanghai Jiao Tong University,  
800 Dong Chuan Road, Shanghai 200240, China*

<sup>6</sup>*Collaborative Innovation Center of Advanced Microstructures, Nanjing University, Nanjing, 210093, China*

We use X-ray tomography to investigate the translational and rotational dynamical heterogeneities of a three dimensional hard ellipsoids granular packing driven by oscillatory shear. We find that particles which translate quickly form clusters with a size distribution given by a power-law with an exponent that is independent of the strain amplitude. Identical behavior is found for particles that are translating slowly, rotating quickly, or rotating slowly. The geometrical properties of these four different types of clusters are the same as those of random clusters. Different cluster types are considerably correlated/anticorrelated, indicating a significant coupling between translational and rotational degrees of freedom. Surprisingly these clusters are formed already at time scales that are much shorter than the  $\alpha$ -relaxation time, in stark contrast to the behavior found in glass-forming systems.

The relaxation dynamics of most disordered materials, such as glass-forming liquids, polymers, foams, granular materials, differs significantly from the Debye behavior found in simple liquids in that it shows a marked non-exponential time dependence [1, 2]. Although several mechanisms can give rise to this type of time dependence, e.g. for polymeric systems it is the chain connectivity, it is often the local disorder of the particle arrangement that is the origin for this behavior [3–5], i.e. the fact that each particle has a different local environment makes that the relaxation dynamics depends strongly on the particle considered. Previous studies have shown that the slowly (or quickly) relaxing particles are not distributed uniformly in space but instead form clusters. This effect, usually named “dynamical heterogeneity” (DH) is nowadays believed to be a key ingredient to understand the  $\alpha$ -process of glass-forming systems, and hence the phenomenon of the glass-transition. As a consequence, many studies have been carried out to study the nature of the DH, in particular how the size of the clusters depends on temperature (or density) of the system [3–11].

Usually DH are associated with the translational degrees of freedom (TDOF) of the particles. The particles in molecular systems and granular materials have, however, also rotational degrees of freedom (RDOF). Since these are coupled with the TDOF it is evident that they will be important for the relaxation dynamics of the system as well [12–16]. However, in practice it is difficult to probe the RDOF in molecular systems since experiments do not allow to track directly the orientation of

individual particles. As a consequence only indirect experimental probing of the RDOF has been possible so far [7, 12] and most of our current knowledge of them comes from computer simulations [17–19]. The situation is not much better for the case of granular materials since these are usually opaque and hence it is very challenging to probe in three dimensions (3d) the displacement and reorientation of the particles [20–26]. Because of the non-spherical shape of the particles and the presence of friction, there is often a strong coupling between the TDOF and RDOF, making the experimental study of the DH for both TDOF and RDOF indispensable for a thorough understanding of the relaxation dynamics [27]. In the present work we thus use X-ray tomography to investigate these DH in a 3d granular packing driven by oscillatory shear, making it to the best of our knowledge the first experimental investigation to probe simultaneously both types of DH.

Our system consists of 4100 hard prolate ellipsoids made of polyvinyl chloride with an aspect ratio of 1.5 (polydispersity 0.9%), i.e. a shape that makes the crystallization of the system difficult [28] and allows for a rather strong T-R coupling. The dimension of the minor axis of the particles is  $2b=12.7\text{mm}$  and in the following we will use  $b$  as the unit of length. The particles are in a rectangular box of dimension  $40.2b \times 43b \times 22.6b$  that can be sheared in the  $y$ -direction. More details of the setup are given in [29]. We drive the system to a steady state by cycling it many times at all strain amplitude  $\gamma$  investigated ( $\gamma = 0.26, 0.19, 0.10,$  and  $0.07$ , see SI for details). Subsequently the position and orientation of all particles are determined by X-ray tomography scans. Scans were made after each complete cycle, thus giving a stroboscopic view of the dynamics with the time unit of one shear cycle, and in the SI we show the mean squared

\* walter.kob@umontpellier.fr

† yujiewang@sjtu.edu.cn

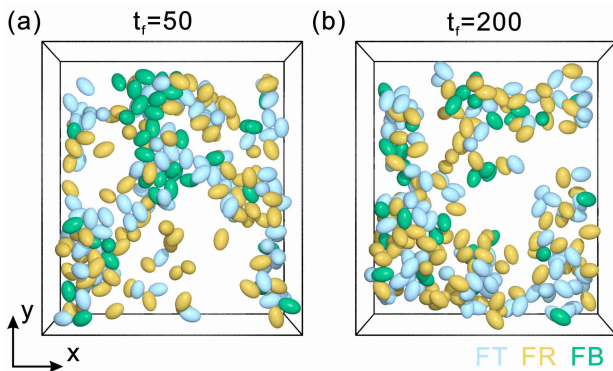


FIG. 1. Snapshots showing the fast translating (FT, blue) and fast rotating (FR, yellow) particles ( $\gamma = 0.10(L)$ ,  $t = 1000$ ). Also shown are the particles that are FT as well as FR (FB, green). Note that both type of particles form clusters and that these clusters overlap significantly. Panels (a) and (b) are for the filter time  $t_f = 50$  and  $t_f = 200$ , respectively.

displacement for the TDOF and the RDOF which allows to get an idea on the relevant time and length scales in the system.

To probe the DH we have tracked the particles for a “filter time”  $t_f$  and determined the distribution of their T- and R-displacements (see SI). Fast (slow) translation particles are defined as the 10% fastest (slowest) particles in this distribution and we denote these particles as FT and ST. The same was done for the RDOF, thus allowing to define the fast (slow) rotating particles, FR and SR. We have verified that the results presented below do not depend in a significant manner on these definitions.

In Fig. 1 we show typical snapshots of the FT and FR particles (blue and yellow, respectively) for two values of the filter time  $t_f$ . One recognizes that both populations form clusters which shows that the T and R dynamics are spatially very heterogeneous. A significant part of the FT particles are also FR (FB, marked in green), indicating that the translational and rotational motion are significantly coupled. Similar conclusions are reached for the slowly moving particles, i.e. the ST and SR (see SI). In the following we will make a quantitative characterization of these DHs.

To determine the cluster size distribution  $P(s)$  of the four populations of particles we define two particles to be neighbors if their Voronoi cells have a common face and use this to construct connected clusters. Figure 2a shows  $P(s)$  for the four populations at different strain amplitudes  $\gamma$  and one recognizes that within the accuracy of the data the curves for different  $\gamma$  coincide, i.e.  $P(s)$  is independent of  $\gamma$ . This somewhat surprising result is likely related to the fact that for granular systems the details of the relaxation dynamics are universal and independent of  $\gamma$  due to the particular manner such systems explore their phase space [29].

Also included in Fig. 2a is a fit to the data with a power-law, a dependence that has been observed in pre-

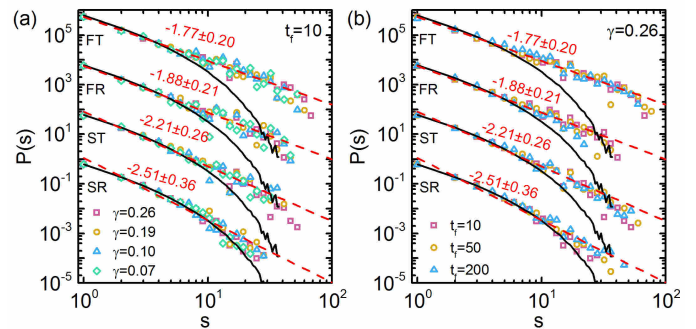


FIG. 2. Cluster size distribution  $P(s)$  for FT, FR, ST, and SR. (The first three sets have been shifted vertically.) The solid black lines are the distributions obtained by randomly picking particles in the system. The dashed red lines are fits to the data with a power-law with exponents stated next to these lines. (a) Different strain amplitude  $\gamma$ . (b) Different filter times  $t_f$ .

vious experiments probing the DH [30]. The exponent is small for the FT clusters and larger for the SR ones (see legend) which shows that the particles with a slow dynamics belong on average to smaller clusters than the FT particles. (The average cluster size are 3.92, 3.16, 2.46, and 2.04 for FT, FR, ST, and SR, respectively.) In the SI we show that the average volume of the Voronoi cell of slow particles is smaller than the one of the fast particles, i.e. the ST and SR clusters are a bit more densely packed than the ones for FT and FR. This shows that fast particles prefer to form extended loose clusters which will allow for cooperative fast motion, similar to the case of glass-forming liquids [10]. Also included in the figure are the  $P(s)$  obtained if one picks 10% of particles in a random manner, i.e. one does not select fast/slow ones. The so obtained average cluster size is 1.94 and the corresponding  $P(s)$ , solid black lines, shows at intermediate and large  $s$  the expected exponential decay, i.e. a  $s$ -dependence that is very different from the power-law that we find for the most/least mobile particles [31].

In Fig. 2b we show  $P(s)$  for  $\gamma = 0.26$  and different values for the filter time  $t_f$  and it is clear that the distribution is also independent of  $t_f$ . Therefore Fig. 2 demonstrates that the DH are independent of the time scale considered, i.e.  $t_f$ , and of the manner the system is driven,  $\gamma$ . This is in contrast to the findings for thermal glass-forming systems in which the DH are usually found to depend on the time scale considered and also on the temperature, i.e. a parameter that is somewhat analogous to our driving strength  $\gamma$ . The surprising fact that clusters are present already at very small  $t_f$ , also confirmed by the observation that the non-Gaussian parameter is basically independent of  $t$  (Fig. SI-13), shows that the DH are *not* related to the  $\alpha$ -relaxation process, in contrast to the findings for thermal glass-formers [10, 19]. Instead, as argued below, we conjecture that it is the surface roughness of the particles that is the source of

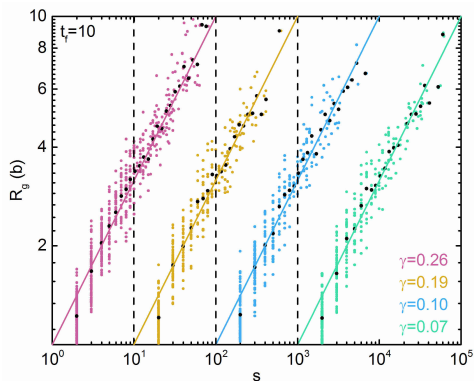


FIG. 3. Radius of gyration of the FT clusters vs  $s$  for different values of  $\gamma$ . Black dots are the average at fixed  $s$ . The solid lines are a guide to the eye with slope 0.5. For the sake of clarity the data for  $\gamma < 0.2$  have been shifted to the right by 10,  $10^2$ , and  $10^3$ .

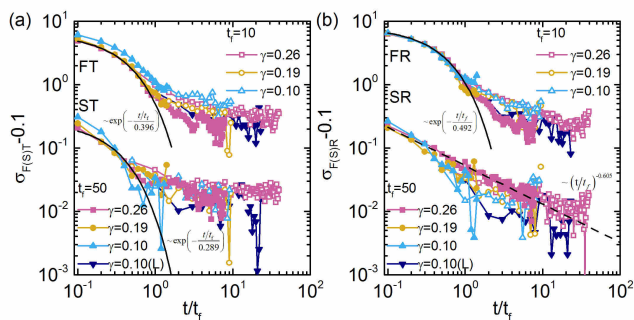


FIG. 4. Probability that a particle that was fast/slow at  $t = 0$  is still fast/slow at time  $t$ . Black solid lines are exponential fits to the data at short times. Panels (a) and (b) are for the TDOF and RDOF, respectively. The data for SR is fitted with a power-law (black dashed line). The FR and SR data has been shifted vertically.

disorder which leads to the DH, i.e. the same mechanism that gives rise to the universal relaxation dynamics observed in Ref. [29].

The cluster size distribution  $P(s)$  is only related to the number of particles in a cluster but contains no information about its geometry. Therefore we determine the radius of gyration  $R_g$  of a cluster via

$$R_g^2 = \frac{1}{s} \sum_{i=1}^s (\mathbf{r}_i - \overline{\mathbf{R}})^2, \quad (1)$$

where  $\mathbf{r}_i$  is the position of particle  $i$  and  $\overline{\mathbf{R}}$  is the center of the cluster. In Fig. 3 we show how  $R_g$  for the FT clusters depends on the cluster size  $s$  and one sees that this dependence is described well by a power-law with an exponent of 0.5, i.e. a mass fractal exponent of 2.0 [32]. This value is independent of the type of particle we consider (FT, FR, ...), see SI, indicating that the geometry of the clusters is independent of the type of motion considered, in contrast to thermal glass-forming systems for

which one finds that the clusters with FT are more open than the ones for ST [33]. Figure 3 also demonstrates that these values are again independent of  $\gamma$ . If we select the particles randomly the resulting mass fractal exponent is around 1.9, i.e. a value that is very close to the one we find for the DH clusters. Hence we conclude that the geometry of the DH clusters is very similar to the one of a random cluster, but that they have an enhanced probability to be large.

The nature of the particles, FT, FR, ..., will change with time and hence it is of interest to probe how long a particle keeps this property since this time can be expected to be related to the life time of the clusters. Therefore we define the quantity  $\sigma_\alpha(t)$  as the probability that a particle which at time  $t = 0$  had a property  $\alpha \in \{\text{FT}, \text{ST}, \text{FR}, \text{SR}\}$  has the same property at time  $t$ . In Fig. 4 we show the  $t$ -dependence of  $\sigma_\alpha$  for the different particles. One recognizes that the curves for the different strain amplitudes fall on top of each other, i.e. the persistence  $\sigma_\alpha(t)$  is independent of  $\gamma$ . This result is surprising since naively one might have expected that a larger strain would lead to a faster loss of memory because for a given fixed time  $t$  the mean squared displacements of the particles increases quickly with  $\gamma$  (see Fig. SI-9) [34]. The figure also demonstrates that the master curve does not depend on the filter time  $t_f$  if one plots the data as a function of the reduced time  $t/t_f$ . This independence shows that the details of the relaxation dynamics do not depend on the time scale considered, i.e. there is a scale invariance of the dynamics in the time window we probe, suggesting that the configuration space explored by the system has a fractal-like nature.

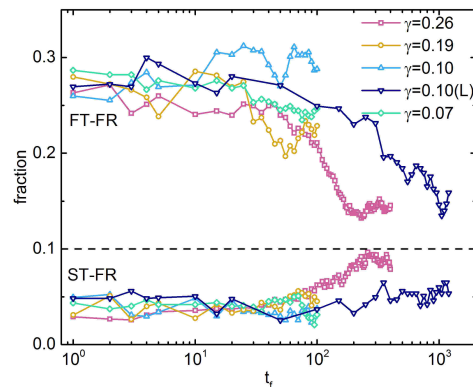


FIG. 5. Probability that a particle is undergoing a FT as well as FR (ST and FR) as a function of the filter time  $t_f$ . The different symbols correspond to different strain amplitudes. The dashed line shows the probability at long times.

Also included in the figure are fits with an exponential function (black solid lines). These fits describe the data well for  $t/t_f \leq 1$  indicating that at short times the particle changes its nature via a simple stochastic escape process. However, for longer times one observes a slower decay: For FR and SR we find a power-law with an exponent around 0.6 whereas for FT and ST the data seems

to go to a finite value given by 0.13 and 0.12, respectively, i.e. the memory does not vanish within the time scale of our experiment. The persistence of this memory regarding the population type of the particle is likely related to the result discussed in Ref. [29] where it was found that the TDOF do show a noticeable memory effect in their motion [35]. From panel (b) we recognize that  $\sigma_\alpha(t)$  for the RDOF shows at intermediate time a power-law with an exponent around 0.6, i.e. there is no plateau, a result that is coherent with the findings that the RDOF show only a rather weak memory in their dynamics [36]. From a physical point of view the absence of a plateau is reasonable since the cycling motion *and the presence of friction* will always lead to a slow rotation of the particles thus permitting them to change their nature (FR or SR).

The persistent rotational motion will induce also a translational motion of the neighboring particles because of steric effects and hence we do expect that friction leads to an enhancement of the rotational-translational coupling [27] which in turn might lead to correlations between the DH of the TDOF with the ones of the RDOF. To study this correlation we determine the overlap between the different clusters, i.e. the probability that a particle simultaneously belongs to two different populations, e.g. FT and FR. In Fig. 5 we show this probability for the combinations FT-FR and ST-FR as a function of  $t_f$ . (Since the definition of the population depends on  $t_f$ , it is clear that the overlap will depend on  $t_f$  as well.) We see that for small and intermediate  $t_f$  the overlap for FT-FR is around 0.27, i.e. by a factor of 2.7 above the trivial value of 0.1 expected for random clusters, and that this enhancement is independent of  $\gamma$ . This implies that there is a significant probability that a particle which is translating quickly is also rotating quickly. For  $t_f$  larger than around  $10^2$  the overlap starts to decay. From the mean squared angular displacement (see Fig. SI-9) one recognizes that this time scale is related to the onset of a significant rotational dynamics, i.e. the particles have rotated far enough that the nature of their rotational dynamics has been randomized, thus leading to a decrease of the overlap. For the case of the ST-FR we see that the overlap is lowered by a factor of two with respect to the trivial value, i.e. slowly translating particles have a significantly reduced probability to rotate quickly, a result that is of course very reasonable. This overlap starts to approach the equilibrium value 0.1 for times that are again on the order of  $10^2$  cycles, i.e. when the particle has rotated by a significant amount (about  $0.5 \text{ rad}^2$ , see Fig. SI-9). In the SI we show, Fig. SI-12, that also the pair ST-SR has an enhanced overlap and the FT-SR has a decreased overlap. None of these overlaps depend on  $\gamma$  if  $t_f$  is not too small and only the decay to the trivial value depends on the driving strength indicating that the decay is indeed related to the randomization of the RDOF.

The presented results show that our granular system

has DH for the TDOF that are qualitatively similar to the ones found in simple glass-forming liquids. Having access for the first time to the RDOF in a 3d experimental system we have probed also the dynamics of the RDOF and we find that also they do show DH with cluster sizes that are just a bit smaller than the ones for the TDOF. The cluster size distribution of all four populations of particles can be described well by a power-law, thus a distribution that is very different from the one of random clusters. Remarkably these distributions are independent of the strain amplitude, indicating that the dynamics is system universal, in qualitative agreement with earlier findings about the van Hove function [29]. The strong correlation and anti-correlation between different types of clusters shows that in this system the translational and rotational degrees of freedom are strongly coupled. This coupling is likely not only caused by the aspect ratio of the particles but also by the presence of friction, an effect that is absent in molecular system.

In Ref. [29] we argued that 3d granular systems show a relaxation dynamics that is very different from the one of thermal glass-formers (e.g. there is no cage effect). Although we now find that the DH are qualitatively similar to the ones of thermal glass-formers, we emphasize that the DH we observe here occur on the time scale that is significantly shorter than the  $\alpha$ -relaxation time, i.e. the time scale at which the particles leave their neighborhood. This surprising observation shows that the energy landscape of granular materials has a structure that is very different from the one of thermal glass-formers since it has a roughness on a length scale that is much smaller than the size of the particles. It can be expected that it is this particle inherent disorder that gives rise to the DH, in contrast to the case of thermal systems in which the variations of the local packing are the cause for the DH. We expect that it is this roughness which makes the properties of the DH to be independent of the driving amplitude and the time scale considered.

In summary we conclude that the presence of DH is not a feature that is unique to thermal glass-formers but instead can be found in other disordered systems as well and hence is more universal than expected. The mechanisms leading to these DH are, however, strongly dependent on the system considered.

## ACKNOWLEDGMENTS

Some of the preliminary experiments were carried out at BL13W1 beamline of Shanghai Synchrotron Radiation Facility. The work is supported by the National Natural Science Foundation of China (No. 11175121, 11675110 and U1432111), Specialized Research Fund for the Doctoral Program of Higher Education of China (Grant No. 20110073120073), and ANR-15-CE30-0003-02.

- 
- [1] K. Binder and W. Kob, *Glassy materials and disordered solids* (World Scientific, Singapore, 2011).
- [2] A. Cavagna, *Phys. Rep.*, **476**, 51 (2009).
- [3] M. D. Ediger, *Ann. Rev. Phys. Chem.* **51**, 99 (2000).
- [4] R. Richert, *J. Phys.: Condens. Matter* **14**, R703 (2002).
- [5] L. Berthier, G. Biroli, J.-P. Bouchaud, L. Cipelletti, and W. van Saarloos, *Dynamical Heterogeneities in Glasses, Colloids, and Granular Media*, Oxford University Press, Oxford, (2011).
- [6] M. M. Hurley and P. Harrowell, *Phys. Rev. E* **52** 1694 (1995).
- [7] M. T. Cicerone, F. R. Blackburn, and M. D. Ediger, *J. Chem. Phys.* **102**, 471 (1995).
- [8] W. K. Kelgel and A. van Blaaderen, *Science* **287**, 290 (2000).
- [9] E.R. Weeks, J.C. Crocker, A.C. Levitt, A. Schofield and D.A. Weitz, *Science* **287**, 627 (2000).
- [10] C. Donati, J.F. Douglas, W. Kob, S.J. Plimpton, P.H. Poole, and S.C. Glotzer, *Phys. Rev. Lett.* **80**, 2338 (1998).
- [11] S. Maccarrone, G. Brambilla, O. Pravaz, A. Duri, M. Ciccotti, J.-M. Fromental, E. Pashkovski, A. Lips, D. Sessoms, V. Trappe, and L. Cipelletti, *Soft Matter* **6**, 5514 (2010).
- [12] I. Chang and H. Sillescu, *J. Phys. Chem. B*, **101**, 8794 (1997).
- [13] C. K. Mishra and R. Ganapathy, *Phys. Rev. Lett.* **114**, 198302 (2015)
- [14] S. Vivek and E. R. Weeks, *J. Chem. Phys.* **147**, 134502 (2017).
- [15] S. H. Chong and W. Kob, *Phys. Rev. Lett.* **102**, 025702 (2009).
- [16] Z. Zheng, R. Ni, F. Wang, M. Dijkstra, Y. Wang, and Y. Han, *Nat. Comm.* **5**, 3829 (2014).
- [17] S. Kämmerer, W. Kob, and R. Schilling, *Phys. Rev. E* **58**, 2141 (1998).
- [18] J. Qian, R. Hentschke, and A. Heuer, *J. Chem. Phys.* **111**, 10177 (1999).
- [19] M. G. Mazza, N. Giovambattista, H. E. Stanley, and F. W. Starr, *Phys. Rev. E* **76**, 031203 (2007).
- [20] D. M. Mueth, G. F. Debregeas, G. S. Karczmar, P. J. Eng, S. R. Nagel, and H. M. Jaeger, *Nature* **406**, 385 (2000).
- [21] P. Richard, P. Philippe, F. Barbe, S. Bourlès, X. Thibault, and D. Bideau, *Phys. Rev. E* **68**, 020301(R) (2003).
- [22] T. Börzsönyi, B. Szabá, G. Törös, S. Wegner, J. Török, E. Somfai, T. Bien, and R. Stannarius, *Phys. Rev. Lett.* **108**, 228302 (2012).
- [23] Y. Fu, Y. Xi, Y. Cao, and Y. Wang, *Phys. Rev. E* **85**, 051311 (2012).
- [24] E. Andò, G. Viggiani, S. A. Hall, and J. Desrues, *Geotech. Lett.* **3**, 142 (2013).
- [25] M. Pica Ciamarra, M. Nicodemi, and A. Coniglio, *Phys. Rev. E* **75**, 021303 (2007).
- [26] M. Harrington, M. Lin, K. N. Nordstrom, and W. Losert, *Granul. Matter* **16**, 185 (2014).
- [27] L. Mohan, K. K. Rao, and P. R. Nott, *J. Fluid Mech.* **457**, 377 (2002).
- [28] A. Donev, I. Cisse, D. Sachs, E. A. Variano, F. H. Stillinger, R. Connelly, S. Torquato, and P. M. Chaikin, *Science* **303**, 990 (2004).
- [29] B. Kou, Y. Cao, J. Li, C. Xia, Z. Li, H. Dong, A. Zhang, J. Zhang, W. Kob, and Y. Wang, *Nature* **551**, 360 (2017).
- [30] A. S. Keys, A. R. Abate, S. C. Glotzer, and D. J. Durian, *Nat. Phys.* **3**, 260 (2007).
- [31] We have also checked that the presented results are independent of the shape of the box considered for the analysis, which show that our results on the cluster size are robust and independent of the details on how they have been obtained.
- [32] Note that in order to determine this exponent we have neglected the clusters of size 2 and 3 since their size is mainly given by local packing geometries (see Fig. SI-8).
- [33] P. Chaudhuri, S. Sastry, and W. Kob, *Phys. Rev. Lett.* **101**, 190601 (2008).
- [34] Note that this independence is qualitatively different from the one discussed in Ref. [29] where it was found that the van Hove function is independent of  $\gamma$  if one rescales the displacement by a  $\gamma$ -dependent factor.
- [35] For times that are well beyond the  $\alpha$ -relaxation time it is clear that  $\sigma_\alpha(t)$  has to go to the trivial values 0.1 since the system will be completely randomized, but these time scales are not accessible in our experiments.
- [36] B. Kou, PhD Thesis, Shanghai Jiao Tong University, 2018.
- [37] GDR Midi, *Eur. Phys. J. E* **14**, 341 (2004).
- [38] C. Xia, K. Zhu, Y. Cao, H. Sun, B. Kou, and Y. Wang, *Soft Matter* **10**, 990 (2014).



## Supplementary Information

### Experimental details

The prolate ellipsoid particles are made of polyvinyl chloride and the 4100 particles, with a total weight of 8.3kg, were poured into the shear cell. A plate that is constrained to move only in the vertical direction was placed on top of the particles. This top plate, with weight of 16kg, provided an extra constant normal pressure of 2.3kPa on the top surface of the packing and thus makes that the pressure gradient in the vertical direction is significantly reduced. During an oscillatory shear cycle, the shear cell will deform to a designed shear strain, then in the opposite direction to the same shear strain and finally return to the origin position. The strain rate for the preparation of the sample and the subsequent measurements is around  $1.7 \cdot 10^{-2} \text{s}^{-1}$  so that the inertial number  $I = 2\dot{\gamma}b/\sqrt{P/\rho}$  is about  $1.4 \cdot 10^{-4}$ , i.e. the experiment can be considered as quasi-static [37]. (Here  $P$  is the pressure and  $\rho$  the mass density.) Before starting the computational tomography (CT) scans we drove the system into a steady state by making hundreds of shear cycles. The number of cycles for the preparation and the subsequent measurements are given in Supplementary Table 1.

Using a medical CT scanner (SOMATOM Perspective, Siemens, Germany), we obtained the complete three-dimensional structural information of the packing with a spatial resolution of 0.6mm. Following similar imaging processing steps as in previous studies, Refs. [29, 38], we determined the position and orientation of each ellipsoid by a marker-based watershed image segmentation technique. We estimated the precision of the position  $\mathbf{r}_i$  and the orientational vector  $\mathbf{e}_i$  of a particle  $i$  by making two consecutive tomography scans of the same static packing and comparing the difference, which gave  $5.3 \cdot 10^{-3}b$  and  $8.4 \cdot 10^{-3}\text{rad}$ , respectively. To avoid the influence of boundary effects, we excluded all particles that have a distance less than  $5b$  from the cell boundary so that we only considered about 1300 central particles for analysis. See Ref. [29] for more details.

To determine the dynamic properties of the system we took a tomography scan after each cycle for the first 10 cycles and then a scan every 5 cycles. For  $\gamma = 0.10$  we made a second experiment in which we scanned only every 50 cycles allowing thus to reach larger times. The so obtained results are labeled as “0.10(L)”.

From the positions and orientations of the particles we calculated their translational displacement as  $\mathbf{d}_j(t) = \mathbf{r}_j(t) - \mathbf{r}_j(0)$  while the rotational displacement was obtained from the time integral of the angular increment of each cycle,  $\boldsymbol{\theta}_j(t) = \int_0^t \boldsymbol{\omega}_j(t') dt'$ , where the modulus and direction of  $\boldsymbol{\omega}_j(t)$  are given by  $\cos^{-1}[\mathbf{e}_j(t) \cdot \mathbf{e}_j(t+1)]$  and the vector  $\mathbf{e}_j(t) \times \mathbf{e}_j(t+1)$ , respectively.

Shear strain (y-direction)	Number of cycles to prepare initial state	Number of cycles for measurements
0.26	300	615
0.19	550	125
0.10	1500	125
0.10 (L)	1500	1850
0.07	2400	125

TABLE I. Experimental protocol used to prepare the system and to make the measurements of its properties.

### Static quantities

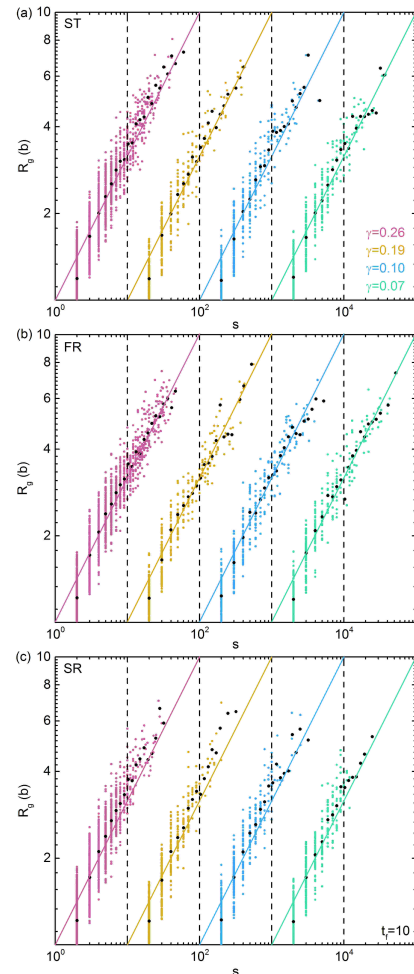


FIG. 6.

Radius of gyration of the clusters as a function of cluster size  $s$  for different values of  $\gamma$ . (a): ST, (b) FR, and (c) SR. The solid lines are a guide to the eye with slope 0.5. Black dots are the average at fixed  $s$ . For the sake of clarity the data for  $\gamma < 0.2$  have been shifted to the right by 10,  $10^2$ , and  $10^3$ .

In Fig. SI-6 we show the relationship between radius of gyration  $R_g$  and cluster size  $s$  for the ST (panel a), FR (panel b) and SR cluster (panel c), which gives an  $s$ -dependence that is very similar to the one of the FT cluster as presented in Fig. 3 of the main text, i.e. a power-law with an exponent close to 2.0. Thus we can conclude that the geometric shape of the clusters is independent of the nature of the particles considered.

In Fig. SI-7 we show the  $t_f$ -dependence of the local volume fraction  $\Phi_{\text{local}}$  for different types of particles.  $\Phi_{\text{local}}$  is obtained by calculating for each particle in the population considered  $\Phi_{\text{local},i} = V_{\text{part}}/V_{\text{Vor},i}$ , where  $V_{\text{part}}$  is the volume of a particle and  $V_{\text{Vor},i}$  is the volume of the Voronoi cell of particle  $i$ , and then taking the average of this ratio over the particles. The graphs show that for  $\gamma = 0.26$ , panel (a), particles with FT and FR have a  $\Phi_{\text{local}}$  that is about 1% smaller than the average, whereas the ST and SR particles have a  $\Phi_{\text{local}}$  that is about 1% higher. Qualitatively the same result is obtained for the strain amplitude  $\gamma = 0.1(L)$ , panel (b), but now the dependence on the type of particle is somewhat weaker. We also note that in both cases the  $t_f$ -dependence is relatively weak, thus showing that, for fixed  $\gamma$ , the filter time does not strongly influence the local packing density of the selected particles.

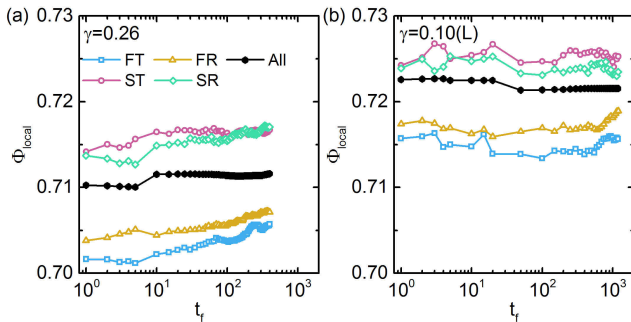


FIG. 7.

The average local volume fraction  $\Phi_{\text{local}}$  for particles that are FT, FR, ST, and ST as a function of the filter time  $t_f$ . Also included is the sample averaged local volume fraction (curve labeled “All”). Panels (a) and (b) correspond to  $\gamma = 0.26$  and  $\gamma = 0.1(L)$ , respectively.

In Fig. 3 of the main text we have shown the radius of gyration of the FT clusters and in Fig. SI-6 the  $R_g$  for the other types of clusters. In Fig. SI-8 we show the corresponding distributions for selected values of the cluster size  $s$ . For very small clusters,  $s = 2$  in panel (a), we see that the distribution has a broad peak with a shape that is directly related to the manner the two particles touch each other (see cartoons of the configurations in the figure). No significant dependence on the cluster type is seen, but a comparison with the distribution of the random clusters (black line) shows that the latter has a slightly more pronounced tail at large  $R_g$ , i.e. configurations in which the particles touch each other at their

tips. That the DH clusters have a less pronounced tail is likely related to the fact that in that geometry (see cartoon) the neighboring particles barely touch and hence friction is not able to couple their motion.

For the case  $s = 3$ , panel (b), we find a double peak structure in the distribution. A closer inspection of the configurations reveals that the peak at smaller distance corresponds to an arrangement in which all three particles touch other two whereas the peak at larger distance to the case in which only two particles touch a central one (see cartoons in the figure). Comparing the distributions for the different cluster types clearly shows that the random cluster has a significantly smaller probability of having three particles touching each other, a result that is very reasonable from the combinatorial point of view and the fact that a tight packing increases the dynamic coupling between the particles. Thus we can conclude that for this cluster size the non-random clusters are more compact than the random ones.

For clusters sizes that are equal or larger than  $s = 4$  the shape of the distribution changes significantly in that it becomes Gaussian like (panels (c) and (d)). We see that also in these cases the random distribution peaks at slightly larger values of  $R_g$ , i.e. the DH clusters are slightly more compact than the random ones. It is also interesting to note that within the accuracy of our data the distribution for the four types of clusters is independent of the mobility of the particles, a result that is consistent with the ones presented in Fig. 3 of the main text and Fig. SI-6.

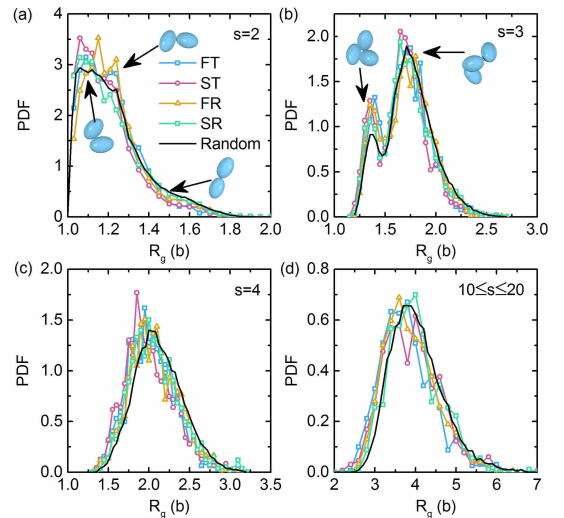


FIG. 8. Probability distribution function of  $R_g$  of FT, ST, FR, SR, and random clusters, for different cluster sizes  $s$ : (a):  $s = 2$ ; (b)  $s = 3$ ; (c)  $s = 4$  (d)  $10 \leq s \leq 20$ .

### Dynamical quantities

To comprehend how far the particles translate and rotate within the time scale of our experiment we show



in Fig. SI-9 (a) and (b) the mean squared displacement of the particles for the TDOF and RDOF, respectively. The data is the same as the one shown in Ref. [29]. Note that the RDOF reach the diffusive limit significantly earlier than the TDOF, i.e. the former are faster than the latter. We also recognize a strong  $\gamma$ -dependence of the data, making the  $\gamma$ -independence of the results shown in the main text rather surprising.

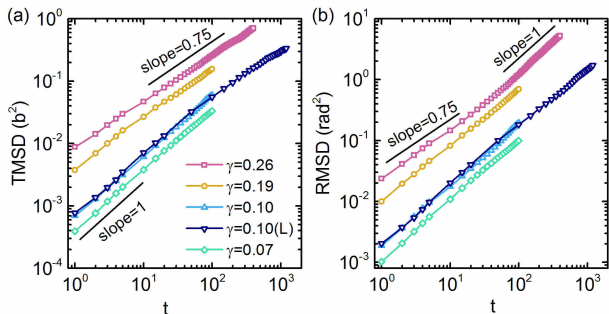


FIG. 9. Time dependence of the TMSD and RMSD for different strain amplitudes  $\gamma$ . Adapted from Ref. [29].

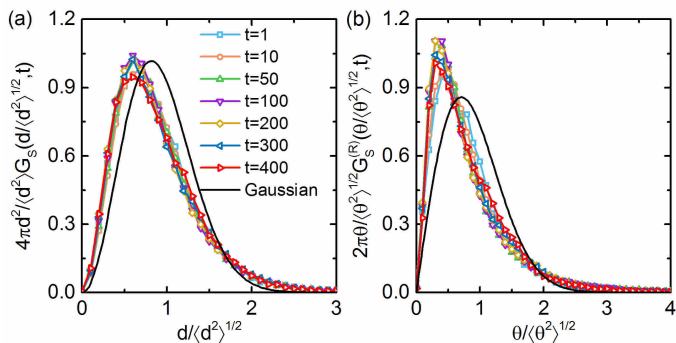


FIG. 10. Self part of the van Hove function for the TDOF and RDOF (panel (a) and (b), respectively) for  $\gamma = 0.26$ . The different symbols are for different times  $t$  and the distance shown on the abscissa is normalized by the corresponding square root of the mean squared displacement. The black solid line corresponds to a Gaussian distribution.

In Fig. SI-10 (a) and (b) we show the self-part of the van Hove function for the TDOF,  $G_s(r, t)$  (see Ref. [29] for its definition), and RDOF,  $G_s^{(R)}(\theta, t)$ , respectively. Here  $G_s^{(R)}(\theta, t)$  is defined as  $G_s^{(R)}(\theta, t) = N^{-1} \sum_{j=1}^N \langle \delta(\theta - |\theta_j(t) - \theta_j(0)|) \rangle$ , where  $N$  is the number of particles and  $\delta$  is the Dirac  $\delta$ -function. The different symbols correspond to different times  $t$ . Note that the abscissa is scaled by the square root of the mean squared displacement at the selected times which makes that the distribution functions fall onto a master curve, a non-trivial result that is discussed in detail in Ref. [29]. Also included in the figures are Gaussians with identical means as the real data (black solid lines). The Gaussians

cross the data at around  $\xi = 1.65(T)$  and  $1.75(R)$ . Thus it is reasonable to define those particles as “fast” that have displacements larger than  $\xi$ . If one integrates the area under the data from  $\xi$  to infinity one gets values between 7.3 and 9.6% i.e. values that are close to the one used in our definition for fast particles, i.e. the top 10% of the distribution. (We mention that we have also repeated the analysis of the cluster size etc. by defining the fast/slow particles as the top/bottom 7% of the distribution and found no significant difference to the results presented in the main text.)

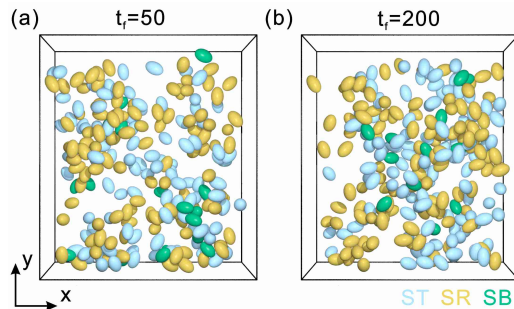


FIG. 11. Snapshots showing the slow translating (ST, violet) and slow rotating (SR, orange) particles for  $\gamma = 0.10(L)$  at  $t = 1000$ . Also shown are the particles that are ST as well as SR (SB, green). Note that both type of particles are forming clusters and that these clusters overlap significantly. Panels (a) and (b) are for the filter time  $t_f = 50$  and  $t_f = 200$ , respectively.

In Fig. SI-11 we show a typical snapshot of the ST and SR particles. (The parameters are the same as the ones of Fig. 1 of the main text.) We see that, as discussed in the main text, also the slowly translating/rotating particles form clusters, i.e. DH, and that these two types of clusters do indeed overlap significantly. This is demonstrated quantitatively in Fig. SI-12 where we show the  $t_f$  dependence of the overlap between ST and SR clusters as well as FT and SR clusters. The former overlap is about 1.5 higher than the trivial values 0.1 whereas the latter is about 50% less than the trivial value. Hence we can conclude that these clusters are clearly correlated/anticorrelated, in agreement with the results from Fig. 5.

Finally we show in Fig. SI-13 the time dependence of the non-Gaussian parameter of the van Hove function for the TDOF, i.e.

$$\alpha_2^{(T)}(t) = \frac{3\langle r^4(t) \rangle}{5\langle r^2(t) \rangle^2} - 1, \quad (2)$$

with an analogous definition for the RDOF. (For the RDOF the factor  $3/5$  has to be replaced by  $1/2$  since the rotational motion is two-dimensional.) We see, panel (a), that for the TDOF  $\alpha_2^{(T)}(t)$  differs significantly from zero already at  $t = 1$ , i.e. the distribution function of the displacements is not a Gaussian, in agreement with the

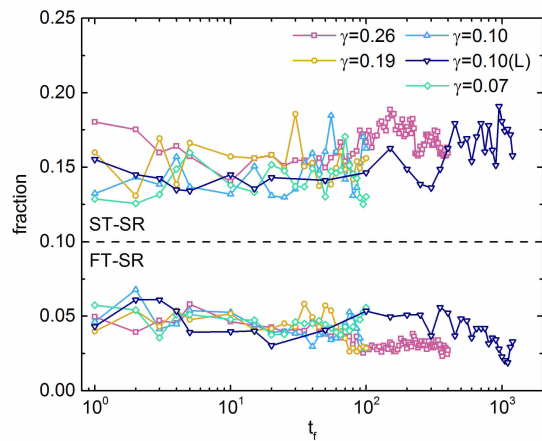


FIG. 12. Probability that a particle is making a ST as well as a SR (FT and SR) as a function of the filter time  $t_f$ . The different lines correspond to different strain amplitudes. The dashed horizontal line shows the random value, i.e. the case that clusters are uncorrelated.

results from Ref. [29]. For larger times  $\alpha_2^{(T)}(t)$  increases slightly, but the  $t$ -dependence remains weak. We also

note that this quantity is independent of the strain amplitude, also this in qualitative agreement with the results presented in Ref. [29]. For the RDOF, we find that  $\alpha_2^{(R)}$  is qualitatively similar to  $\alpha_2^{(T)}$  except that the data is more noisy, see panel (b).

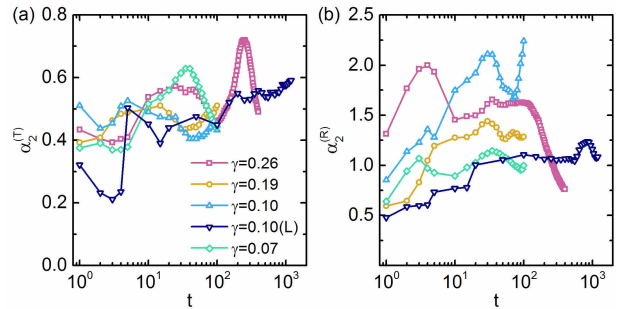


FIG. 13.

Time dependence of the non-Gaussian parameter  $\alpha_2(t)$  for the TDOF, (a), and the RDOF, (b), for different strain amplitudes  $\gamma$ .